ANDRZEJ KAWALEC[*], JERZY WIKTOR[**]

ANALYSIS OF STRENGTH OF TOOTH ROOT WITH NOTCH AFTER FINISHING OF INVOLUTE GEARS

Computer simulation of involute spur gears generation was used to determine tooth profiles mapped by tools during gear machining. These profiles were computed for different combinations of geometric parameters of machined gears and tools as well as for different combinations of pretreatment and finishing processes. Results of simulations were used for generation of very precise finite element models of representative gear segments. For these models, distributions of stresses were computed for assumed load in the ADINA finite element system. The results were compared with related results of computations made in accordance with the ISO/DIS and AGMA standards. Special attention was paid to gears, in which additional notch appears at tooth root after machining. This notch causes concentration of stresses. On the basis of the above named computations an analysis of influence of technological parameters and methods of machining gears on form and bending strength properties of spur gear tooth root was performed. General conclusions were formulated. They can be useful in both gear design and gear manufacturing for proper selection of structural parameters, association of pretreatment and finishing, selection of suitable method of gear generation and parameters of applied tool. Approach suggested in this paper: setting initial structural and technological parameters, computer simulation of gear generation, computer assisted strength analysis leading to suitable modification of the design and manufacturing presumptions – establishes proper basis for optimization of gears with consideration to the maximum possible bending strength properties of spur gear tooth root.

1. Introduction

One of the most frequent reasons for failure of any gearing is immediate or fatigue breakage of tooth. Such failure, usually, limits gear transmission

---

[*] *Faculty of Mechanical Engineering and Aeronautics, Rzeszów University of Technology, W. Pola 2, 35-959 Rzeszów, Poland; E-mail: ak@prz.rzeszow.pl*

[**] *Faculty of Mechanical Engineering and Aeronautics, Rzeszów University of Technology, W. Pola 2, 35-959 Rzeszów, Poland; E-mail: jwiktor@prz.rzeszow.pl*

durability because tooth breakage results in cutting off the link between driving shaft and related shaft being driven. This is especially dangerous in the case of gear transmissions used in aviation. Therefore, special attention must be paid to analysis of gear tooth strength for breakage.

Usually, tooth fracture starts from *tooth fillet* on stretched side of loaded tooth and develops along its root. Therefore, stress distribution at tooth root, especially at tooth fillet, gives some representative information for evaluation of tooth root strength for breakage [7], [6], [11], [12], [19].

Stresses at tooth root can be approximately calculated with use of the procedures given in corresponding standards ISO/DIS [11], DIN [6] and AGMA [2]. Precise computation of stress distribution requires application of experimental methods (like measurements with the use of electric resistance wire strain gauges [23] or photo-elastic measurements [18], [23]) as well as numerical methods (e.g., finite element method [3], [16], [21] or use of bipotential equations, utilizing Airy function [17], [18]).

2 Tooth fillet and fillet profile

Tooth fillet is a surface connecting involute tooth flank (where tooth contact takes place) with root surface (Fig. 1). Structural and technological parameters of this surface (shape, radius of curvature, structure of the outer layer, roughness, etc.) significantly influence strength properties of tooth root.
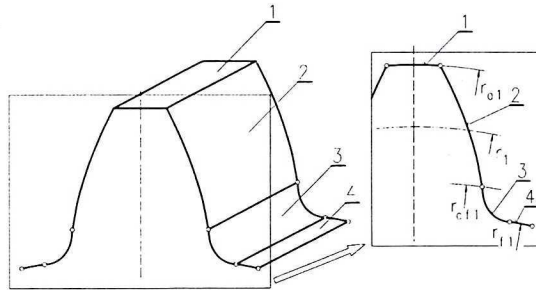
Fig. 1. Boundary surfaces of spur gear tooth flank: 1 - tooth tip surface (segment of cylindrical surface), 2 - involute or helix-involute tooth flank surface, 3 - tooth fillet, 4 - bottom land of gear-root surface (segment of cylindrical surface) (left); Tooth profile in end face of tooth section: 1 - tooth tip (an arc of tooth tip circle), 2 - tooth flank (segment of involute), 3 - tooth fillet profile, 4 - bottom land of gear-root arc (an arc of the bottom land of gear circle) (right)

Geometric and strength analyzes of spur gearings are usually performed for plain (normal or transverse) sections of teeth. Therefore, instead of fillet surface - *fillet profile*, normal or transverse, is considered. It results from sectioning representative tooth with normal surface or transverse surface, respectively (Fig. 1). Tooth fillet profile depends on both structural factors (module, number of gear teeth, angle of tooth profile, addendum modification coefficient) and technological parameters (type and geometric parameters of tool for

pretreatment, association of pretreatment and finishing processes, etc.) [15]. Depending on particular combination of the above named factors, different tooth fillet profiles can be generated during gear manufacturing (Fig. 2):

- *single-part tooth fillet profile* – appears when tooth flank and tooth fillet are machined simultaneously (in one technological operation) with tool without protuberance (an exception from this rule is the case of machining gear with lower number of teeth than limiting number, when undercut of tooth root turns up);
- *tooth fillet with undercut* – can appear like unexpected result of undercut at tooth root in the case of machining gears with lower number of teeth than limiting number or like desired effect, when tool with protuberance is used for gear machining (in order to eliminate notch at tooth root after grinding of gear);
- *tooth root fillet with notch* – appears in the case when, after pretreatment made with tool without protuberance, in separate technological operation only involute tooth flank profile is finished by grinding, honing or shaving (due to the negative influence of grinding on strength properties of gear tooth, i.e. wheel burns, grinding of both tooth fillet and root surfaces is usually omitted).
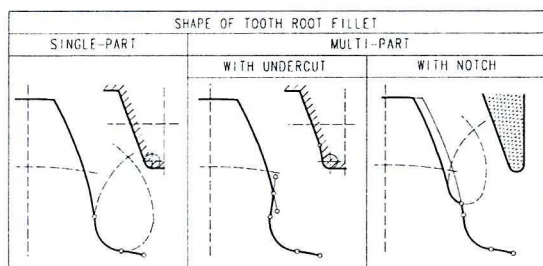
Fig. 2. Types of tooth root fillet

Notch at tooth root can appear also in the case, when special tool with protuberance is used for pretreatment. In this case notch can turn up at tooth root in result of:

- improper setting of finishing tool;
- excessive deformations following heat treatment preceding finishing of gear;
- considerable errors of pitch, established during pretreatment of gear [17].

3. Tooth fillet profile - geometric notch

Nominal stress in particular section of machine part, loaded with arbitrary force or moment is usually calculated by dividing the load by the area of the section or by its section module. In the case of parts with changing sections

(parts with geometric notches) concentration of stresses occurs. It means significant enlargement of stresses in surrounding of places where rapid changes of section appear (Fig. 3).
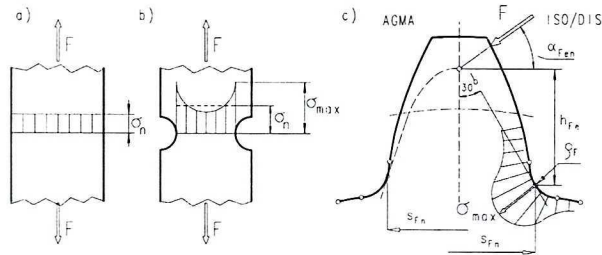
Fig. 3. Concentration of stresses caused by geometric notch: a) structure without notch; b)structure with geometric notch; c) involute tooth with tooth root fillet - geometric notch; critical section at tooth root according to the AGMA and ISO/DIS standards [2], [11]

In approximate calculations notches can be considered by application of corresponding coefficients, used like multipliers of nominal stresses [5], [25]. For precise computations of stresses more detailed analysis is necessary and is usually made with use of experimental or numerical methods e.g., with finite or boundary elements.

The most important factors influencing stress concentration are: shape and dimensions of particular notch (especially its depth and radius of curvature), material properties, heat treatment, state of outer layer of the notch (roughness, machining marks, etc.), working temperature and stress state in the notch. Concentration of stresses caused by notch can be characterized by *stress concentration coefficient* α_k. This coefficient equals ratio of maximum stresses which occur in notch σ_{max} to nominal stresses σ_n in considered section (Fig. 3) [5], [24], [25]:

$$\alpha_k = \frac{\sigma_{max}}{\sigma_n} \tag{1}$$

Real structural materials are not so sensitive to notches, like it could follow from stress concentration coefficient α_k (Eq. 1). Therefore, in calculations additional coefficient – *notch performance factor* β_k is considered. This factor is determined in experimental fatigue investigations of structures. During such investigations strength of samples with notch is compared with strength of related samples (the same cross-section and the same material) without notch. In the case of bending, notch performance factor β_k is calculated from the following formula:

$$\beta_k = \frac{Z_{gc}}{Z_{gck}} \tag{2}$$

where Z_{gc} and Z_{gck} denote strength for fatigue bending of smooth sample and sample with notch, respectively. In the case of strength analysis of gears, gear-shape samples are used for experimental investigations of their fatigue.

In order to link the coefficients α_k and β_k together, additional coefficient – *coefficient of notch performance sensitivity* η_k is introduced:

$$\eta_k = \frac{\beta_k - 1}{\alpha_k - 1} \tag{3}$$

Tooth fillet constitutes a typical geometric notch. Therefore, computation of stresses at tooth root requires considering stress concentration in it. Known methods of stress calculation depend on type of tooth fillet. In practice, usually, discrete methods are used, due to their flexibility in geometric modelling and ability of considering different non-linearities of the models.

Gears possess geometric symmetry. Therefore, only certain segment of gear with suitable boundary conditions applied to it can represent the whole gear. Moreover, in the case of spur gears, both straight tooth and helical, the 3D model of gear tooth is an outline of the 2D profile moved along a vector parallel to the axis of symmetry of a gear without (straight tooth gears) or with continuous rotation (helical gears). If attention in strength analysis is focused on contact stresses at tooth flank, then of course the 3D finite element model with the whole tooth flank should be considered due to specific non-uniform distribution of contact stress along tooth trace and profile. In such 3D model both distribution of load and tooth contact area should be determined with consideration to several geometric and mechanical factors including also stiffness of teeth, gears, shafts, bearings, etc. [14], [22]. On the other hand, if attention is focused on tooth-root stress caused by load applied either at tooth tip (as it is the case of investigations described in this paper) or at the highest point of single tooth contact then, considering that except the loads at tooth flank there are no lads and stresses acting at the external faces of the gear, the problem can be analyzed as a plain stress problem [2], [11] due to its geometry, loads and boundary conditions. In such model the loads should be calculated according to its unit width. It should be noted that in the case of helical gearings real helical gear is replaced with virtual one with virtual number of teeth and load applied in the transverse section [2], [11].

Numerical computations of stress distribution based on finite elements, presented in this work, required precise modelling of tooth shape and finite element mesh for more than 150 finite element models. Therefore, specialized mesh generating program, linked with the ADINA [1], was developed to allow parametric and automatic generation of well-shaped finite element meshes for plain stress problems with consideration to proper node numbering and required tooth fillet profile [13], [15].

Considering geometric symmetry of each gear only certain gear segments were defined and used for FEM computations. They represented plain stress models and were made of the eight-node isoparametric plain stress finite elements. All nodes at the internal circle of gear rim in the above named models had all degrees of freedom fixed. In addition to this, the nodes at both radial boundary sections had all degrees of freedom fixed, except the related radial

movements defined in their local coordinate systems (Fig. 4). The models were loaded at tooth tip with corresponding prescribed force (Fig. 4). The finite element meshes of the loaded tooth precisely reflected tooth profile after gear manufacturing. Three characteristic examples of the finite element meshes generated at tooth root (in accordance with assumed gear manufacturing processes) are shown in Fig. 5.
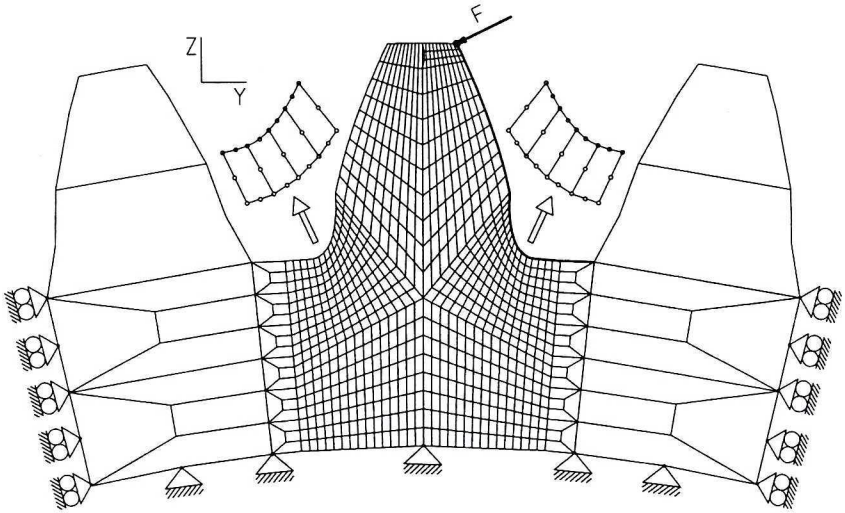
Fig. 4. The finite element model of a segment of a gear with force applied at tooth tip
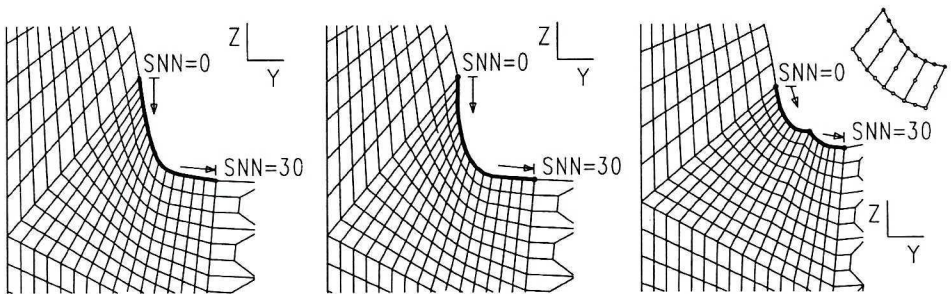
Fig. 5. Examples of finite element meshes for considered kinds of tooth root shapes: single-part tooth fillet profile (left), tooth root with undercut (middle), tooth root with notch arising after finishing (right); SNN - serial node number (used in some further graphs)

In order to investigate influence of mesh density on computed stresses and trace convergence of the results, three types of models with various mesh densities at tooth root representing the same fillet with notch were generated and used for the finite element calculations. All models were made of the eight-node isoparametric plain stress finite elements. Stresses obtained in the case of 43 and 61 nodes at the fillet, respectively, are compared with the basic model –

sample of the models used throughout the whole paper, i.e. with the model containing 31 nodes at the fillet. Some details concerning considered meshes and the results are given in Tab. (1).

Table 1.

General quantitative data describing the meshes based on the eight-node isoparametric plain stress finite elements and used for stress caculations of the considered gear segments with notch.

No. of elements	No. of nodes	No. of nodes at the fillet	$\sigma_{eff.\,max}$, MPa
829	2610	31	314.706
937	2946	43	313.435
1099	3450	61	314.185

Distributions of the effective stresses computed along tooth fillet for the above named models with notch and differences in the effective stresses (computed with the models containing 31 and 61 nodes at the fillet, respectively) related to the average and maximum calculated tooth-root stresses in the basic model with 31 nodes at the fillet are shown in Fig. 6.
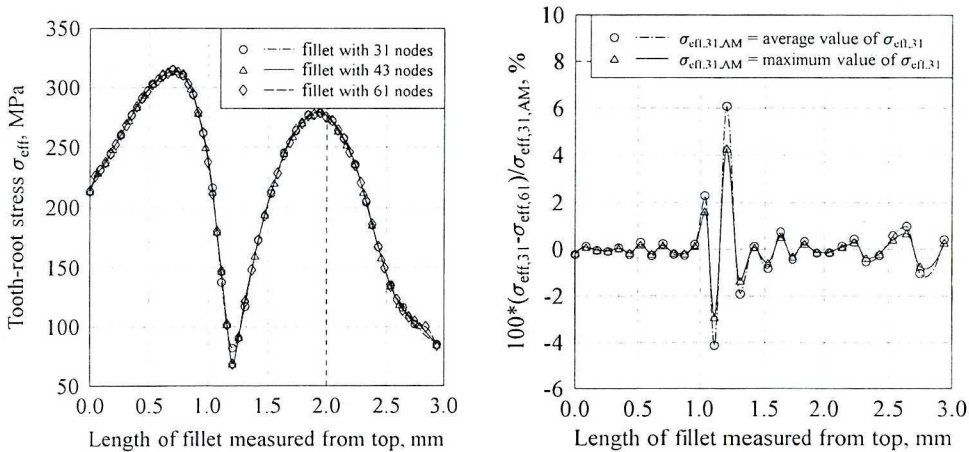
Fig. 6. Distributions of the effective stresses computed along tooth fillet with notch for the models with different mesh densities described in Tab. 1 (left), and differences in the effective stresses (computed for the models containing 31 and 61 nodes at the fillet, respectively) related to the average and maximum calculated tooth-root stresses in the basic model with 31 nodes at the fillet (right)

From Tab. 1 and Fig. 6 it follows that effective stress calculated in the considered models with various mesh densities differ form each other not more than 6% (related to the maximum effective stress $\sigma_{eff.\,max}$ computed for the basic model, described in the first row of the Tab. 1). At the same time, the maximum effective stress $\sigma_{eff.\,max}$ calculated in the considered models with various mesh densities differ form each other not more than 0.4% (Tab. 1).

4. Stresses at tooth root

4.1. Single-part tooth fillet

Contact force acting at tooth flank causes complex stress state at tooth root, including bending, compression and tangent stresses. To characterize the effort at tooth root it is necessary to compute effective stresses in accordance with one of the known strength hypotheses. Concentration of stresses depends on type and profile of tooth fillet and especially on radius of its curvature. Typical distribution of effective stresses at tooth root with single-part fillet is shown in Fig. 7. Stresses are calculated with use of the finite element method (FEM), applied in the ADINA finite element system [1].
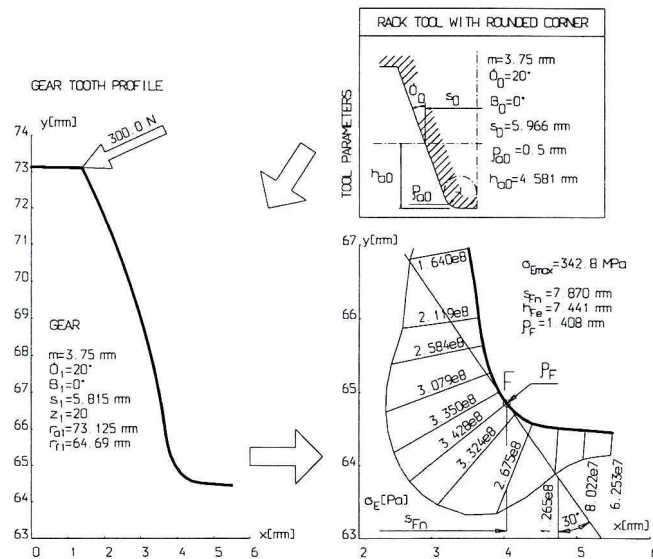
Fig. 7. Distribution of stresses at tooth root with single-part tooth root fillet; critical section at tooth root according to the ISO/DIS standard [11]

As follows from Fig. 7, stresses at tooth root increase in direction towards the root, achieve maximum in certain *critical section* and then decrease. Maximum stresses calculated at the critical section are considered as representative stresses for evaluation of tooth bending strength. Two different methods of calculation of location of the critical section and stresses in the critical section are given in ISO/DIS [11] and AGMA [2] standards (Fig. 3). Formulas applied in both standards and results of calculations are given and compared in [8], [9], [10].

4.1.1 Calculation of stresses at tooth root in accordance with the ISO/DIS standard

According to the ISO/DIS standard [11], location of the critical section is determined by point F – point of tangency of the fillet with a straight line

inclined with $30°$ to the tooth center line (Fig. 3). Nominal stress in this section σ_{F0} are calculated from the following formula:

$$\sigma_{F0} = \frac{F_t}{bm_n} Y_F Y_S Y_\beta \tag{4}$$

where: F_t – transmitted tangential load at the pitch diameter; b – effective face width; m_n – normal module; Y_F – tooth form factor (taking into account influence of shape of fillet on stresses at tooth root); Y_S – stress correction factor (considering concentration of stresses in result of existence of notch at the fillet and complex stress state, i.e. bending, compression and shear); Y_β – helix angle factor (giving consideration to influence of helix angle on tooth-root stresses in helical gears).

Multiplying the nominal stress in the critical section σ_{F0} by the load factors, considering non-uniform distribution of loads and additional dynamic loads acting in gear transmission, local tooth-root stress is obtained:

$$\sigma_F = \sigma_{F0} K_A K_v K_{F\alpha} K_{F\beta} \tag{5}$$

where: K_A – application factor for bending strength (considering variation of gear transmission load due to external factors); K_v – dynamic factor for bending strength (considering increase of load due to external factors); $K_{F\alpha}$ – transverse load factor (root stress); $K_{F\beta}$ – face load factor (root stress); both load factors consider non-uniform distribution of load between teeth pairs and along path of contact, respectively.

The objective of this work was in analysis of influence of shape and geometric parameters of tooth fillet on stresses at tooth root. Therefore, it was assumed, that load is uniformly distributed in gear transmission and there are no other dynamic internal or external loads acting. Therefore, all factors which are not directly linked with geometry of tooth and gear were omitted in presented analysis.

Tooth form factor Y_F can be calculated from the formula:

$$Y_F = \frac{6(h_{Fe}/m)\cos\alpha_{Fen}}{(s_{Fn}/m)^2 \cos\alpha} \tag{6}$$

where: h_{Fe} – bending moment arm; α_{Fen} – load angle; s_{Fn} – tooth thickness at the critical section (Fig. 3).

According to the ISO/DIS standard, coefficient Y_F considers influence of tooth shape on stresses at tooth root. However, like it follows from Eq. (6), this coefficient takes into account only one geometric parameter of tooth fillet, i.e. tooth thickness in the critical section, and angle of contact force.

Concentration of stresses caused by tooth fillet is considered by application of the stress correction factor Y_S which corresponds to the shape coefficient α_k given in Eq. (1). In the case of single-part fillet without additional notch resulting from finishing, this coefficient is calculated from the formula [11]:

$$Y_S = (1.2 + 0.13L)q_s^{(1.21+2.3/L)^{-1}} \tag{7}$$

where:

$$L = \frac{s_{Fn}}{h_{Fe}} \qquad (8)$$

and

$$q_s = \frac{s_{Fn}}{2\rho_F} \qquad (9)$$

Variables s_{Fn}, h_{Fe} and ρ_F in Eqs. (8), (9) denote tooth thickness in the critical section, arm of bending force and radius of curvature of tooth fillet at the critical section, respectively (Fig. 3).

From Eq. (7) follows, that in calculations of Y_S coefficient only two geometric parameters of tooth fillet, determined at the critical section, are taken into account - s_{Fn} and ρ_F. Therefore, computation of stresses at tooth root in accordance to the ISO/DIS standard considers only two geometric parameters calculated at only one section - the critical section. In the case of single-part fillet results obtained with use of Eq. (4) are, however, comparable with related results of experimental investigations (made with electric resistance wire strain gauges or photo-elastic models) [24] as well as with results of numerical computations performed with the FEM and the ADINA finite element system [1].

Sample results of calculations of nominal tooth-root stress according to the ISO/DIS standard for models of gears with single-part tooth fillet are given in Figs. (8), (9). They are compared with the related nominal tooth-root stress calculated according to the ANSI/AGMA standard and with the maximum effective von Mises tooth-root stress computed with the use of the ADINA finite element system [1]. Figure (8) contains results obtained for different numbers of teeth z_I and Fig. (9) – for different magnitudes of the load angle α_I. In both cases, gears generated with racks with rounded tip were considered.
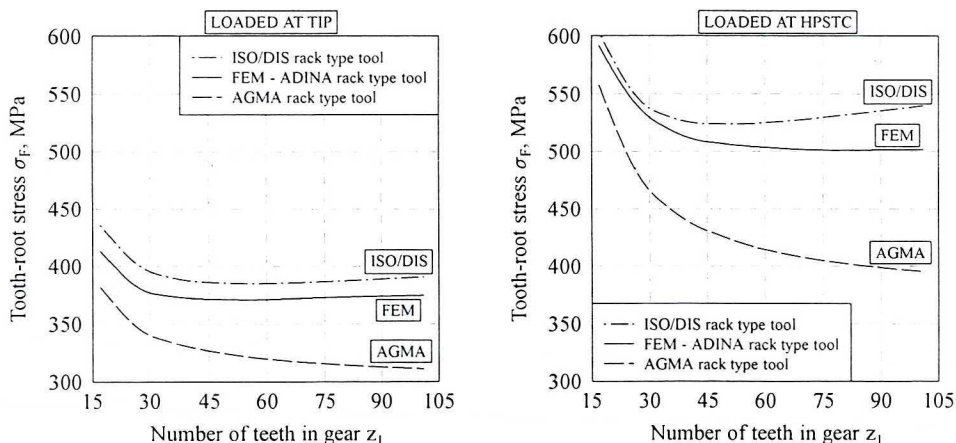
Fig. 8. Influence of the number of gear teeth z_I on tooth-root stress σ_F according to the ISO/DIS standard, AGMA standard and FEM: for load applied at the tip (Tip) $F_{bn}/b = 250$ N/mm (left) and for load applied at the HPSTC $F_{bn}/b = 500$ N/mm (right); main parameters of the rack (generating tool): $\alpha_0 = 20°$, $s_0 = 4.320$, $h_{fP} = 1.22\ m_n$, $\rho_{fP} = 0.18\ m_n$; main parameters of the gear: $m_n = 2.75$, $\alpha_I = 20°$, $s_I = 4.265$, $\beta_I = 0°$

Figure 9 presents distribution of effective loads along a single-part fillet for gears with different magnitudes of the load angle α_l. Stresses were computed with the use of the ADINA finite element system.
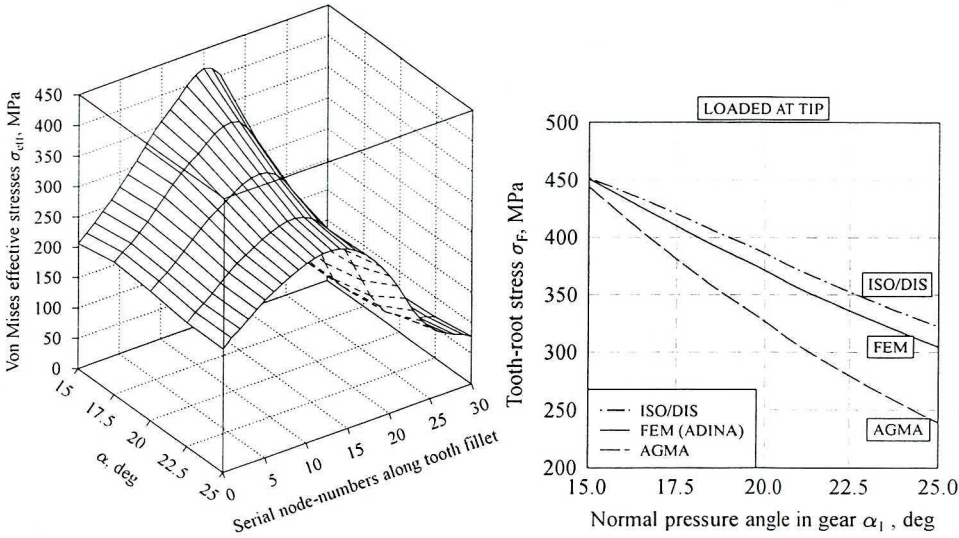
Fig. 9. Distribution of stresses at tooth root along the single-part fillet (serial node numbers SNN are shown in Fig. 5) for different load angles α_l (left) and influence of the load angle α_l on tooth-root stress σ_F according to the ISO/DIS, AGMA and FEM: for load applied at the tip (Tip) $F_{bn}/b = 250$ N/mm; main parameters of the gear: $m_n = 2.75$, $z_l = 45$, $s_l = 4.265$, $\beta_l = 0°$; main parameters of the rack (generating tool): $s_0 = 4.320$, $\rho_{fP} = 0.18\, m_n$ (right)

4.1.2. Calculation of stresses at tooth root in accordance with the ANSI/AGMA standard

According to the ANSI/AGMA standard [2] location of the critical section is determined by point F – point of tangency of the constant strength parabola with the fillet (Fig. 3). Nominal stress σ_{F0} at the critical section is calculated from the formula:

$$\sigma_{F0} = \frac{F_{wt}}{bm_n} \frac{1}{J} = \frac{F_{wt}}{bm_n} \frac{K_f}{Y} \frac{m_N}{C_\Psi} \tag{10}$$

where: F_{wt} – transmitted tangential load at the operating pitch diameter; J – bending strength geometry factor; K_f – stress correction factor; Y – tooth form factor; m_N – load sharing ratio (for spur gears $m_N = 1.0$; for helical gears $m_N = b/L_{min}$); C_Ψ – helical overlap factor (for spur and conventional helical transmissions $C_\Psi = 1.0$).

Multiplying the nominal stress in the critical section σ_{F0} by the load factors, local tooth-root stress is obtained:

$$\sigma_F = \sigma_{F0} K_a K_s K_m K_v^{-1} \tag{11}$$

where: K_a – application factor for bending strength; K_s – size factor for bending strength (considers influence of size of gearing on tooth-root stress); K_m – load

distribution factor for bending strength; K_v – dynamic factor for bending strength.

Similarly to the ISO/DIS standard, an influence of shape of tooth (including parameters of the fillet) on tooth-root stress is taken into consideration by application of the tooth form factor, given by the following formula:

$$Y = \cos\beta_w \cos\beta \left[\frac{\cos\alpha_{Fen}}{\cos\alpha_{wn}} \left(\frac{6h_{Fe}}{s_{Fn}^2 C_h} - \frac{\tan\alpha_{Fen}}{s_{Fn}} \right) \right]^{-1} \tag{12}$$

where: α_{Fen} – load angle; α_{wn} – operating normal pressure angle; β – helix angle at the reference cylinder; β_w – operating helix angle; C_h – helix factor.

Concentration of stresses caused by fillet is taken into account by application of the stress correction factor K_f:

$$K_f = H + \left(\frac{s_{Fn}}{\rho_F} \right)^L \left(\frac{s_{Fn}}{\rho_{Fe}} \right)^M \tag{13}$$

where:

$$H = 0.331 - 0.436\alpha_n, \qquad L = 0.324 - 0.492\alpha_n, \qquad M = 0.261 + 0.54\alpha_n$$

Exemplary results of calculations of the nominal tooth-root stress made in accordance with the ANSI/AGMA standard are shown in Figs. 8, 9.

4.2. Tooth fillet with undercut

According to the ISO/DIS and ANSI/AGMA standards, maximum stresses at tooth root with a small intentional undercut, resulting from application for pretreatment a tool with protuberance, could be approximately calculated from formulas given in Eqs. (5)–(9), like in the case of single-part tooth fillet. However, an influence of undercut on tooth thickness s_{Fn} in the critical section should be considered.

In the ISO/DIS standard the magnitude of undercut s_{pr} is taken into account in calculations of the auxiliary coefficient E:

$$E = \frac{\pi}{4} m_n - h_{fP} \tan\alpha_n + \frac{s_{pr}}{\cos\alpha_n} - (1 - \sin\alpha_n) \frac{\rho_{fP}}{\cos\alpha_n} \tag{14}$$

Coefficient E is used for calculation of parameters of the critical section, which are linked with calculations of tooth-root stress.

In the ANSI/AGMA standard [2] the magnitude of undercut s_{pr} (here denoted δ_{a0}) is used in calculation of an angle to center "S" of tool tip radius λ_{ns}. Similarly to the coefficient E in the ISO/DIS standard, the angle λ_{ns} is used for calculations of parameters of the critical section and tooth-root stress:

$$\lambda_{ns} = 2\left(\text{inv}\phi_{np0} - \text{inv}\phi_{ns} + \frac{\delta_{a0} - \rho_{a0}}{r_{nb0}} \right) \tag{15}$$

Distribution of stresses at tooth root with undercut, computed with the FEM, are shown in Fig. 10. Comparison of these results with the results obtained in

the case of teeth without undercut (Fig. 7) shows, that distributions of stresses are similar to each other. Small undercut does not cause additional effect of stress concentration. Slight increase of stresses results from smaller tooth thickness s_{Fn} at tooth root. In the example shown in Fig. 10 stresses were approximately 7% bigger than in the case of single-part tooth fillet.
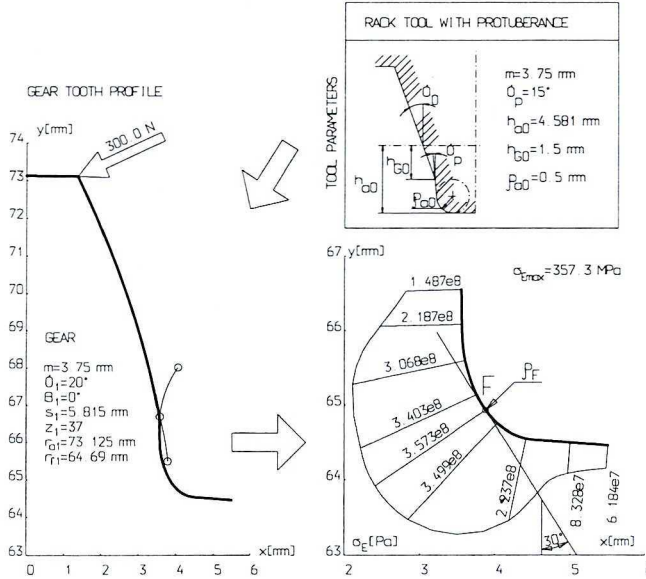
Fig. 10. Distribution of stresses at tooth root with undercut

4.3. Tooth fillet with notch

In the case when tooth root and tooth flank are machined separately in two different operations an additional notch appears (Fig. 11). It takes place, when after gear pretreatment (during which tooth fillet is formed) finishing (shaving, grinding or honing) is applied only to tooth flank. Then two geometric notches turn up (Fig. 11), one notch after finishing (notch I) and the other one – tooth fillet (notch II). Each of them causes local stress concentration. They also interact mutually with each other.
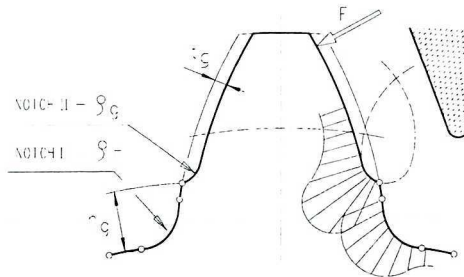
Fig. 11. Tooth root fillet with notch after finishing; geometric parameters of the notch; distribution of stresses at tooth root

Distribution of stresses at tooth root depends on location and geometric parameters of notches (depth of notch after finishing, distance from tooth root, radii of curvature of both notches). Typical distribution of stresses at tooth root in the case of tooth fillet with notch is shown in Fig. 12.
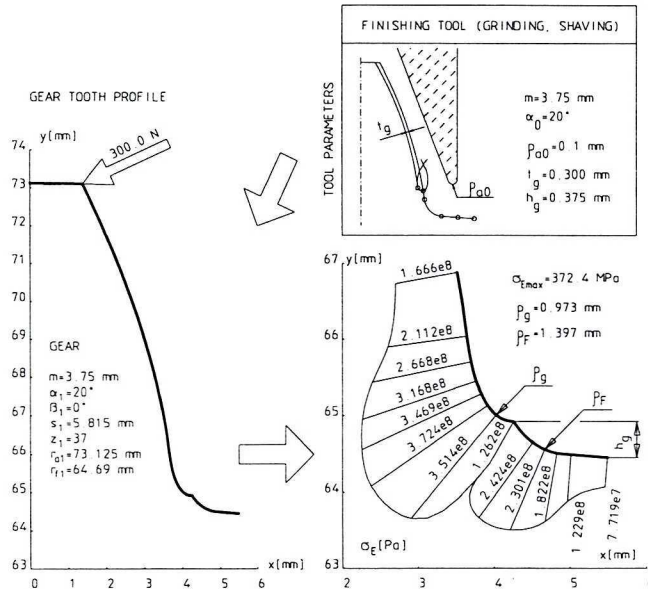
Fig. 12. Distribution of stresses at tooth root with notch

From Fig. 12 follows, that there are two local maxima of stresses, reflecting the notches. Tooth thickness in surrounding of the notch after finishing is significantly less than tooth thickness in the critical section of tooth fillet. Radius of curvature of notch after finishing ρ_g is usually less than corresponding radius of curvature of tooth fillet ρ_F (Fig. 11). This causes, that stresses at notch II (Fig. 11) are usually greater than stresses in other parts of tooth root. However, in certain cases (for suitable combination of geometric parameters of both notches) the notch after finishing can relieve stresses, decreasing maximum stresses at tooth root.

Lower strength of tooth root with notch after finishing results from not only geometric reasons. In the case of gears after grinding tooth root with notch is additionally weakened due to a negative influence of grinding process on strength, especially fatigue strength (negative effects associated with wheel burns).

Problem of stress distribution at tooth root with single-part tooth fillet was investigated in details in both experimental and analytical ways [19], [24]. On the basis of obtained results certain procedures were established, allowing approximate determination of the maximum stresses at tooth root and location of the critical section [11], [20], [7]. In the case of tooth fillet with notch after finishing distribution of stresses is more complex and neither results nor formulas developed for single-part tooth fillet can be applied directly. For this

type of tooth fillet additional investigations must be performed.

The ISO/DIS standard [11] describes the procedure for approximate evaluation of strength of tooth root with notch (in the ANSI/AGMA standard [2] this type of fillet is not taken into account). The stress correction coefficient Y_S, considering concentration of stresses in result of existence of notch and complex stress state (bending, compression and shear), is replaced in formula for maximum stresses at tooth root with single-part tooth fillet (Eq. 5), with coefficient Y_{sq}, which considers existence of additional notch at tooth root:

$$Y_{sq} = \frac{1.3Y_s}{1.3 - 0.6\sqrt{t_g/\rho_g}} \qquad (16)$$

where: t_g – maximum depth of notch after finishing (Fig. 11) and ρ_g – radius of curvature of notch after finishing (Fig. 11).

Coefficient Y_{sq} takes into account only two parameters of notch: notch thickness t_g and radius of curvature ρ_g. It does not consider other important parameters influencing stresses, like distance of notch from tooth root h_g, radius of curvature of tooth fillet ρ_F, mutual interaction of both notches. Equation (5) allows to calculate stresses in only one section. Precise analytic determination of stress distribution at tooth root, considering all important geometric parameters of tooth fillet, requires application of more complex methods for strength computations.

Detailed analysis of stress distribution at tooth root with notch after finishing is given in [18]. It is based on biharmonic equations utilizing Airy function [17]. Results of calculations were experimentally verified with photo-elastic measurements as well as on pulsators. Influence of the most important parameters of gearing and geometric parameters of notch on distribution and maximum stresses at tooth root were also analyzed there. Numerical method used in [17] required continuous profile. Therefore, stresses were calculated not for real tooth profile but for virtual profile, in which tooth tip and sharp connection of notch with tooth fillet were replaced with circular arcs. Another simplification of the models used in [17] consisted in assuming rectilinear tooth profiles of rack applied for gear generation. Such simplification of the models used for computations could have, however, significant influence on the obtained results.

In this work an analysis of influence of all important geometric parameters characterizing tooth root on stresses and their distribution, especially at tooth root, was performed. Strength computations were made with the FEM and the ADINA finite element system [1] for real tooth profiles i.e., for tooth profiles mapped during generation with particular tools with assumed geometric parameters. Both kinematics of gear generation and association of pretreatment with finishing processes were considered. Tooth profiles were computed by computer simulation of gear generation described in details in [15]. Results of the finite element analysis of gears were compared with results obtained according to the ISO/DIS standard for the corresponding models of gears. Some of them are shown in Figs. 14, 16, 21, 23.

5. Influence of structural and technological parameters of gearing on stresses at tooth root with notch after finishing

The following structural and technological parameters were considered in strength analysis of tooth root stress in this work:

- distance of notch from tooth root h_g;
- notch depth after finishing t_g;
- tip radius of tool used for pretreatment ρ_{aoI} (this parameter determines tooth fillet profile at tooth root, especially radius of curvature of the notch ρ_F);
- tip radius of tool used for finishing ρ_{aoII} (this parameter determines profile of the notch at tooth root, especially its radius of curvature ρ_g);
- number of gear teeth z_I;
- addendum modification coefficient x;
- nominal angle of tooth profile α.

An influence of tooth module on stresses at tooth root is well known. Therefore, it was not investigated in this work. In all computations it was assumed, that both tooth module and contact force are constant for all considered models in order to have a common basis for comparing the results.

5.1. Distance of notch from tooth root h_g

Influence of distance of notch from tooth root h_g on distribution of stresses at tooth root in both notches is shown in Figs. 13, 14. Both graphs were done for the parameter h_g related to the module of gearing h_g/m. For small values of h_g
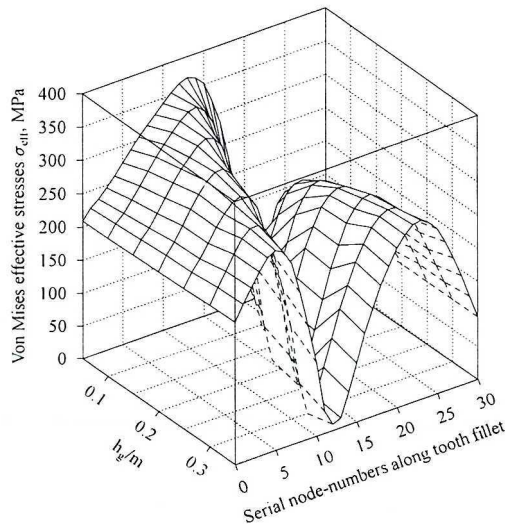
Fig. 13. An influence of the distance of the notch after finishing from tooth root of a gear h_g/m on the distribution of stresses at tooth root
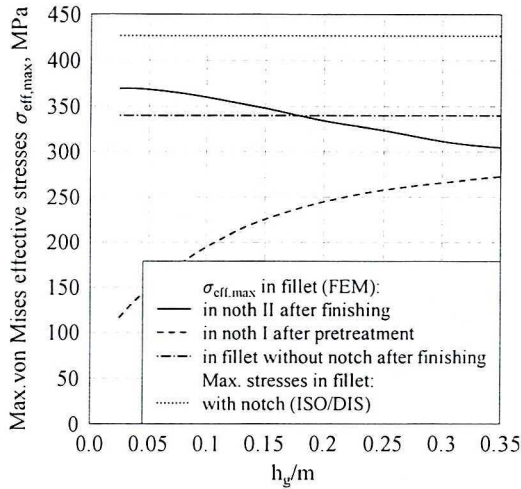
Fig. 14. An influence of the distance of the notch after finishing from tooth root of a gear h_g/m on the maximum stresses at tooth root in notch I (tooth root fillet after pretreatment) and in notch II (tooth root fillet after finishing)

maximum stresses in notch after finishing are significantly bigger than stresses at tooth fillet. They are also bigger than maximum stresses in tooth root in the case of single-part tooth fillet. With increasing distance h_g stresses in notch after finishing diminish and then, in surrounding of tooth fillet, amplify again. In the example shown in Fig. 14 an increase of parameter h_g/m from 0.025 to 0.35 caused deducting of maximum stresses at tooth root by approximately 17%.

Computations have shown, that with big distance of notch form tooth root (i.e., for $h_g/m > 0.175$ in Fig. 14) the notch after finishing acts like deducting notch. Maximum stresses at tooth root are then less than in the case of single-part tooth fillet. The distance h_g cannot be freely expanded, however, because it shortens active involute profile at tooth root and can lead to tooth contact disturbances during work of gear transmission.

5.2. Notch depth after finishing t_g

Notch depth after finishing t_g results from machining allowance for finishing of tooth flank (Fig. 11). An influence of this parameter on distribution of stresses at tooth root and on maximum stresses is shown in Figs. 15 and 16, respectively.

With increasing notch depth after finishing t_g maximum stress in notch after finishing slightly grows. At the same time, stresses in surrounding of tooth fillet decline (e.g., increase of parameter t_g from 0.1 to 0.4 magnifies maximum stress in notch after finishing by 4.5%). Maximum stresses in both notches computed for different combinations of parameters h_g and t_g are shown in Figs. 17, 18, 19.
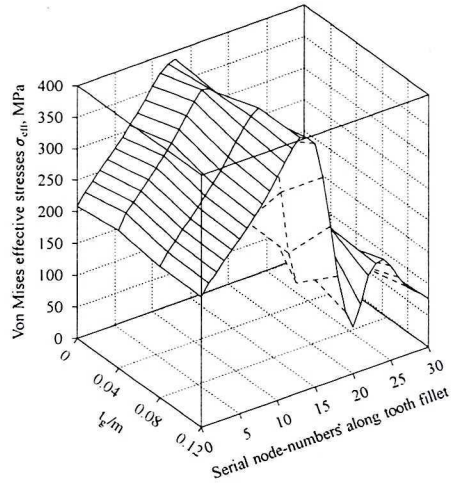
Fig. 15. An influence of the depth of the notch after finishing t_g/m on the distribution of stresses at tooth root
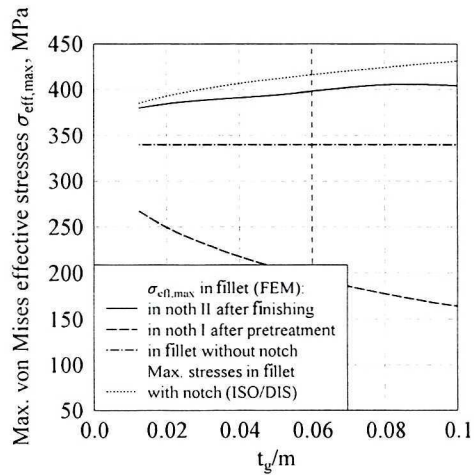
Fig. 16. An influence of the depth of the notch after finishing t_g/m on the maximum stresses at tooth root in notch I (tooth root fillet after pretreatment) and in notch II (tooth root fillet after finishing)

From presented graphs follows, that stresses are influenced not only by considered parameters h_g and t_g separately, but also by their combination. Minimum stresses in notch I appear for big value of the distance h_g and small notch depth t_g. Simultaneously, minimum stresses in notch II appear for small value of the distance h_g and big notch depth t_g.
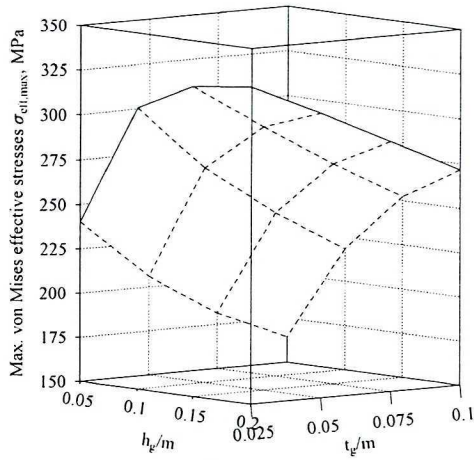
Fig. 17. An influence of the distance of the notch after finishing from the bottom land of a gear h_g/m and the depth of the notch after finishing t_g/m on the maximal stresses at tooth root in notch I (tooth root fillet after pretreatment)
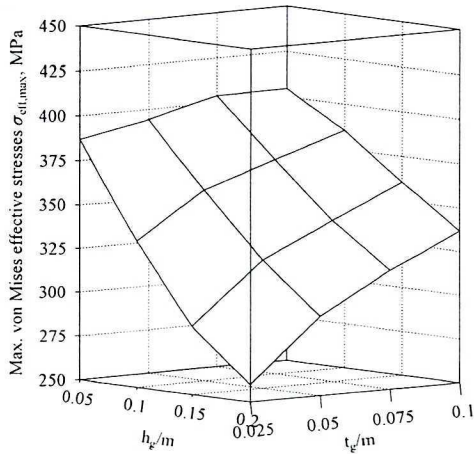
Fig. 18. An influence of the distance of the notch after finishing from tooth root h_g/m and the depth of the notch after finishing t_g/m on the maximum stresses at tooth root in notch II (tooth root fillet after finishing)
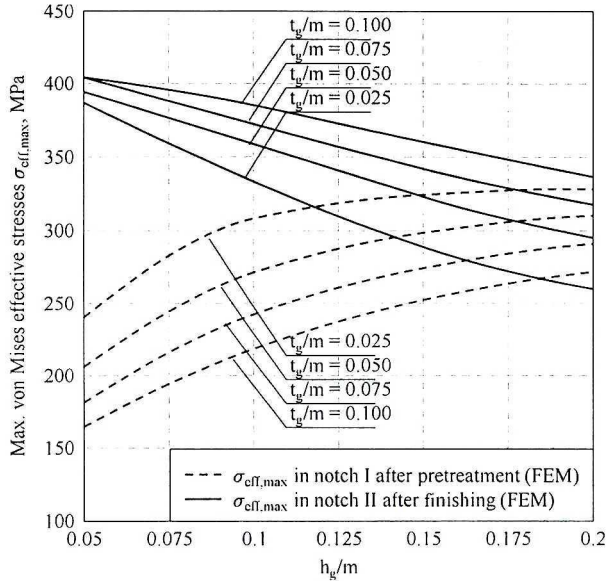
Fig. 19. An influence of the distance of the notch after finishing from tooth root h_g/m and the depth of the notch after finishing t_g/m on the maximum stresses at tooth root in notch I (tooth root fillet after pretreatment) and in notch II (tooth root fillet after finishing)

5.3. Tip radius of tool used for pretreatment ρ_{ao1}

Tooth fillet results from gear generation as an envelope of subsequent locations of cutting edge of tool tip. The profile of this curve and radius of curvature of tooth fillet at the critical section ρ_F depend on type of tool used for pretreatment and on tip radius of the tool ρ_{ao1}. This relation was described in [15].
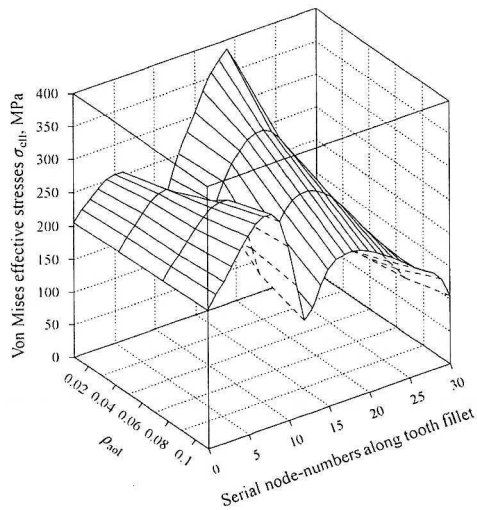
Fig. 20. An influence of the tip radius of the tool used for pretreatment ρ_{ao1} (related to the tooth-root fillet radius ρ_{FI}) on the distribution of stresses at tooth root
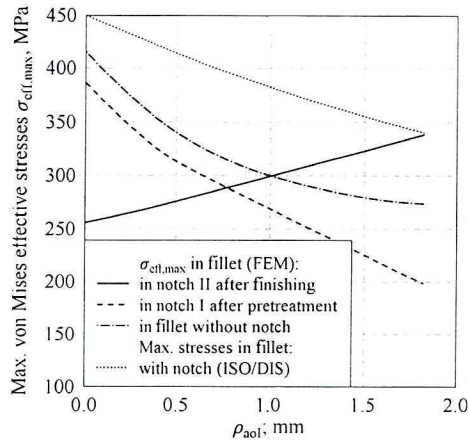
Fig. 21. An influence of the tip radius of the tool used for pretreatment ρ_{aoI} (related to the tooth-root fillet radius ρ_{FI}) on the maximum stresses at tooth root in notch I (tooth root fillet after pretreatment) and in notch II (tooth root fillet after finishing)

Therefore, the radius ρ_{aoI} significantly influences distribution of stresses at tooth root both in surrounding of tooth fillet and in notch after finishing (effect of interaction of both notches). Relation between the radius ρ_{aoI} and stresses in tooth root is shown in Figs. 20, 21.

For small values ρ_{aoI} bigger stresses occur in surrounding of tooth fillet. With increasing ρ_{aoI} these stresses decline, but stresses in notch after finishing grow. For the certain value of ρ_{aoI} stresses in both notches are equal. This value of the radius ρ_{aoI} provides minimum stresses at tooth root and, in result, maximum bending strength of tooth. In the example shown in Fig. 21 stresses at tooth root are lower than stresses calculated for the case of $\rho_{aoI} = 0$ by approximately 30%. With the radius ρ_{aoI} growing further bigger stresses appear in notch after finishing than in tooth fillet.

Stresses which occur in tooth with notch are matched with maximum stresses in tooth of corresponding gear with the same main geometric parameters (generated with the same tool) and single-part tooth fillet. Comparison shows, that for small values ρ_{aoI} maximum stresses in tooth root with notch are slightly lower than stresses in tooth root with single-part tooth fillet. This conclusion applies only to geometric parameters and does not consider negative influence of finishing, especially grinding, on tooth root strength.

5.4. Tip radius of tool used for finishing ρ_{aoII}

Notch at tooth root, which appears after gear generation, is formed by cutting edge of finishing tool tip (tip of grinding wheel, shaving cutter or honing tool), like it is in the case of tooth fillet after finishing. Profile and radius of curvature of the notch ρ_g depends on type of finishing tool and on its tip radius ρ_{aoII}. The radius ρ_{aoII} influences stresses in notch after finishing and their distribution. Both

geometric notches at tooth root interact with each other. Therefore, the radius ρ_{aoII} determines stresses at tooth root. This relation is shown in Figs. 22, 23.
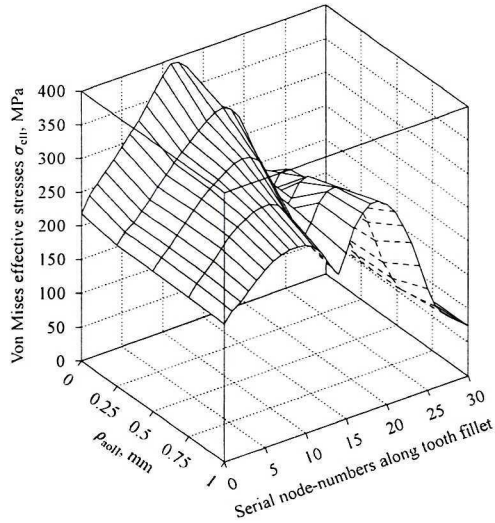
Fig. 22. An influence of the tip radius of the tool used for finishing ρ_{aoII} (related to the radius of curvature at notch II ρ_{FII}) on distribution of stresses at tooth root
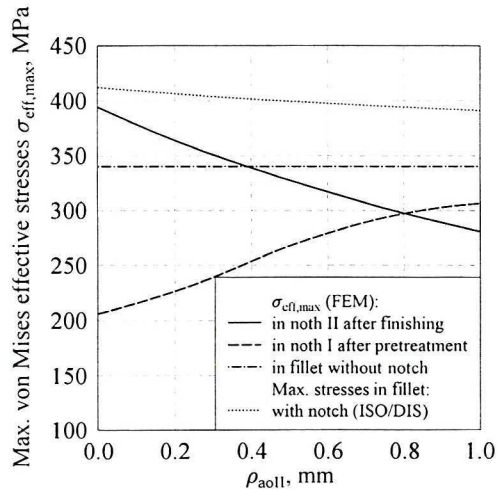
Fig. 23. An influence of the tip radius of the tool used for finishing ρ_{aoII} (related to the radius of curvature at notch II ρ_{FII}) on the maximum stresses at tooth root in notch I (tooth root fillet after pretreatment) and in notch II (tooth root fillet after finishing)

For small values of the radius ρ_{aoII} stresses in notch are significantly bigger than stresses in surrounding of tooth fillet. With growing radius ρ_{aoII} the corresponding radius of notch after finishing magnifies and stresses in the notch decline. Stresses at tooth fillet simultaneously grow. For certain value of the radius ρ_{aoII} the curves reflecting stresses in both notches intersect and maximum

bending strength is obtained. Similarly, like in the case of the radius ρ_{aoI}, further amplification of the radius ρ_{aoII} causes enlargement of maximum stresses in tooth root. Difference between maximum stresses in tooth root for $\rho_{aoII} = 0$ and for optimal value of the radius ρ_{aoII} was in considered example (Fig. 23) approximately 25%.

Interaction of both notches at tooth root (the radii ρ_{aoI} and ρ_{aoII}) on maximum stresses in tooth root is shown in Figs. 24, 25, 26.
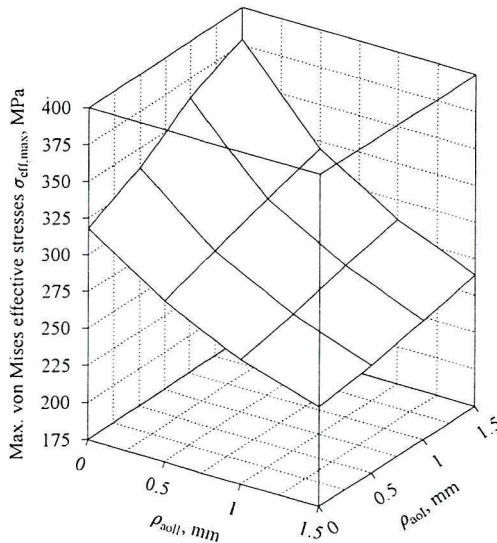
Fig. 24. An influence of the tip radii of the tools used for pretreatment ρ_{aoI} and for finishing ρ_{aoII} on the maximum stresses at tooth root in notch I (tooth root fillet after pretreatment)
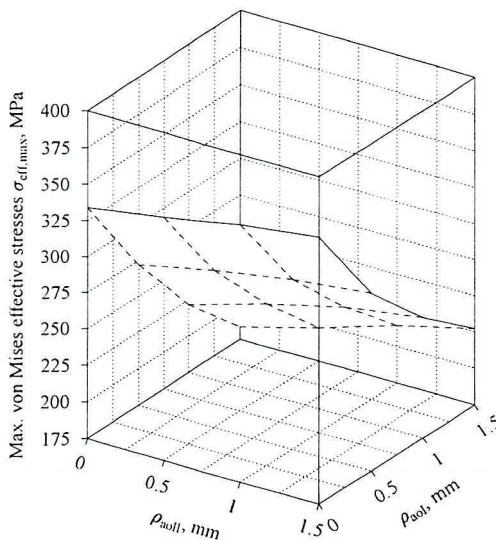
Fig. 25. An influence of the tip radii of the tools used for pretreatment ρ_{aoI} and for finishing ρ_{aoII} on the maximum stresses at tooth root in notch II (tooth root fillet after finishing)
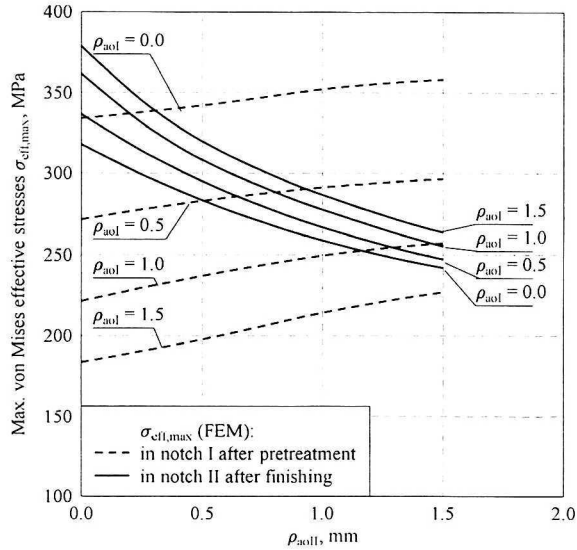
Fig. 26. An influence of the tip radii of the tools used for pretreatment ρ_{aoI} and for finishing ρ_{aoII} on the maximum stresses at tooth root in notch I (tooth root fillet after pretreatment) and in notch II (tooth root fillet after finishing)

5.5. Number of gear teeth z_I

Changing number of gear teeth z_I leads to changes in profile of tooth fillet after gear generation and profile of notch after finishing. It follows change of cylinder, around which generating tool rolls during gear machining. In order to investigate influence of such change in both profiles on tooth root, strength computations were done for gears with different number of teeth varying between 17 and 57. Results are shown in Figs. 27, 28.
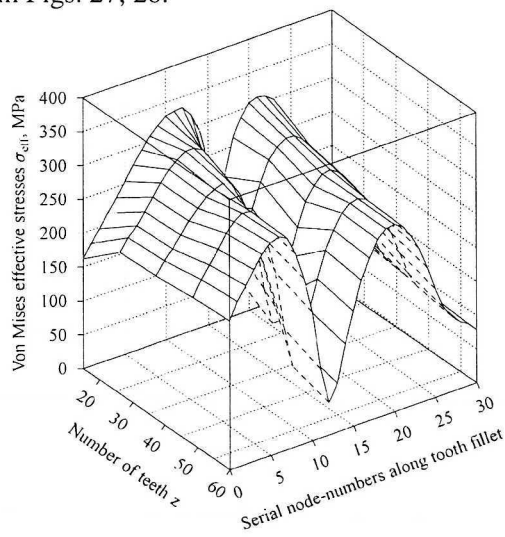
Fig. 27. An influence of the number of teeth z on the distribution of stresses at tooth root with notch after finishing
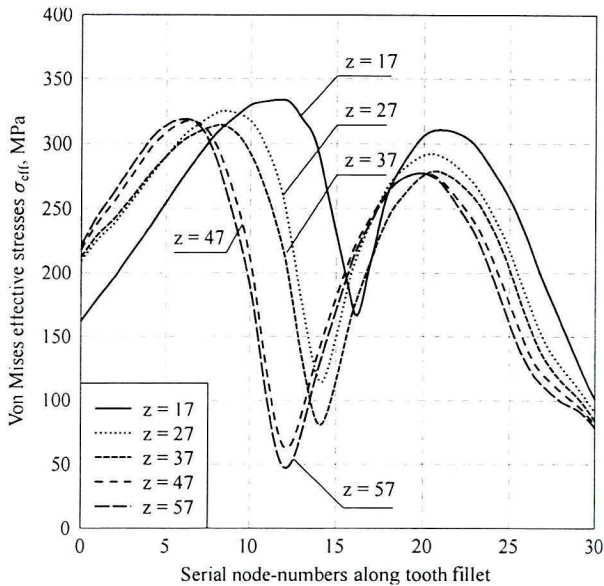
Fig. 28. An influence of the number of teeth z on the maximum stresses at tooth root in notch I (tooth root fillet after pretreatment) and in notch II (tooth root fillet after finishing)

Change in the number of gear teeth z_i influences first of all location of maximum stresses (location of the critical section). It does not significantly influence their maximum value. In the considered example change of maximum stresses calculated for the range from $z_i = 27$ to $z_i = 57$ was approximately 3%. Only in the case of small number of gear teeth $z_i = 17$ a slight increase of maximum stresses was observed. It is related to undercut of tooth root, which turns up during gear generation.

5.6. Addendum modification coefficient x

Addendum modification forces slight change in tooth root shape both in surrounding of notch after finishing and tooth fillet. It is generally caused by change in location of generating tool in relation to machined gear during both pretreatment and finishing processes. Results of computation of stresses at tooth root performed for finite element models of gears with different values of the addendum modification coefficient x are shown in Figs. 29 and 30.

Presented results show, that addendum modification influences only location of the critical section, like it is in the case of change in number of gear teeth z_i. Addendum modification does not significantly influence maximum stresses in the notches. In the example shown in Figs. 29 and 30 the difference in maximum stress for the addendum modification coefficient x changing between $x = -0.3$ and $x = 0.3$ was approximately 4%.
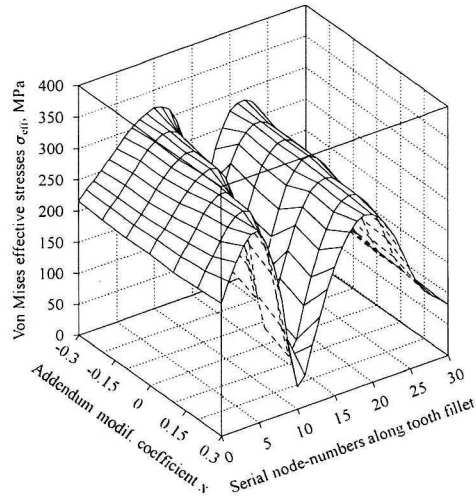
Fig. 29. An influence of the addendum modification coefficient x on distribution of stresses at tooth root with notch after finishing
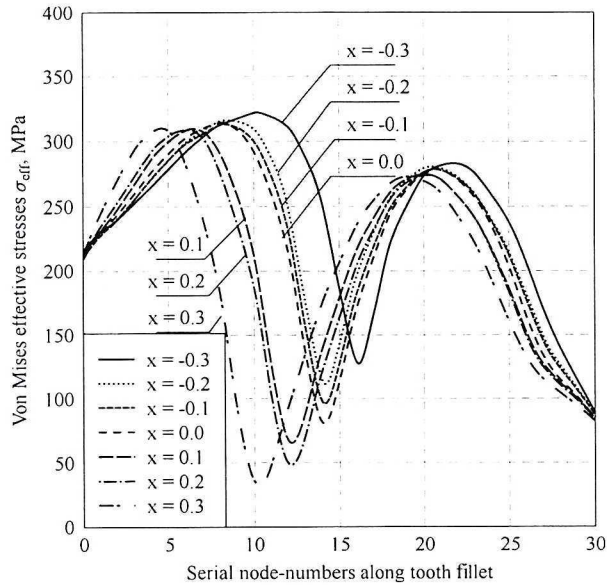
Fig. 30. An influence of the addendum modification coefficient x on the maximum stresses at tooth root in notch I (tooth root fillet after pretreatment) and in notch II (tooth root fillet after finishing)

5.7. Nominal angle of tooth profile α

Nominal angle of tooth profile α influences both gear tooth profile and tooth thickness at tooth root. Distributions of stresses were computed for five different values of the nominal angle of tooth profile α varying in the range between $\alpha = 15°$ and $\alpha = 25°$. Results of computations are shown in Figs. 31 and 32.
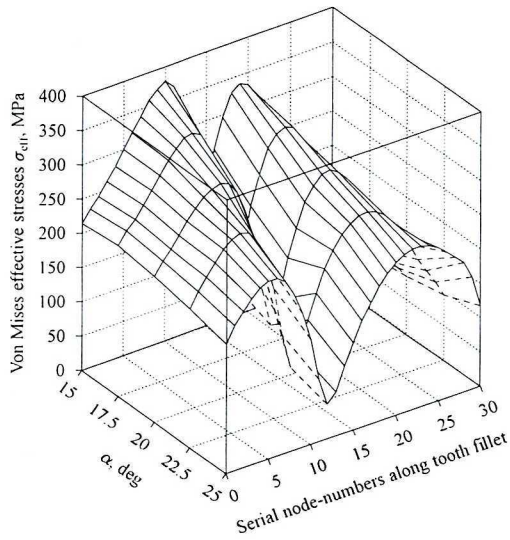
Fig. 31. An influence of the angle of tooth profile α on the distribution of stresses at tooth root with notch after finishing
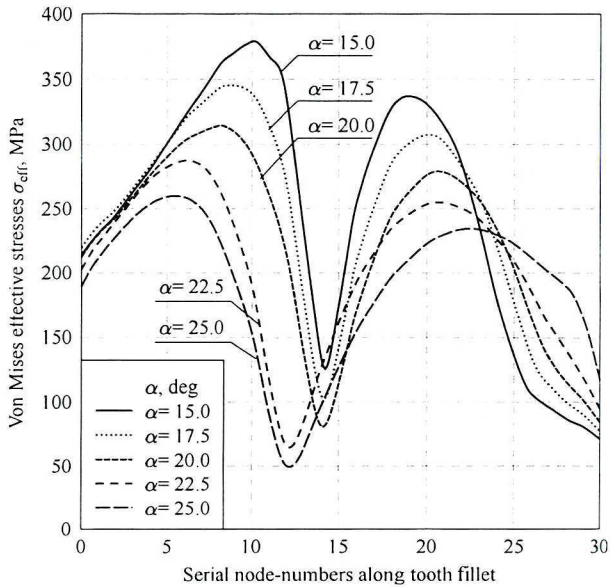
Fig. 32. An influence of the angle of tooth profile α on the maximal stresses at tooth root in notch I (tooth root fillet after pretreatment) and in notch II (tooth root fillet after finishing)

From obtained results it follows, that from all three parameters considered: z_1, x and α, the angle of tooth profile α has the most significant influence on tooth root strength. With growing angle α maximum stresses in notch after finishing and in surrounding of tooth fillet significantly reduce (Figs. 31, 32). It follows first of all from growing tooth thickness at tooth root. In examples

shown in Figs. 31 and 32 difference in maximum stresses in tooth root computed for extreme values of the angle of tooth profile α was above 30%.

6. Conclusions

In this work analysis of influence of the most important geometric parameters of gearing, especially type and parameters of tooth fillet, on stresses and their distribution at tooth root in tooth loaded with contact force is presented. Stresses were calculated with the finite element method for the finite element models of segments of gears (Figs. 4, 5). Results of FEM computations were compared with stresses calculated in accordance with procedures described in ISO/DIS and AGMA standards. Three types of tooth fillet, which can occur after gear machining (Fig. 2), were considered. Tooth profile of machined gear depends on parameters of tool. Therefore, radii of curvature of tooth fillet ρ_F and notch ρ_g were defined through related radii of tools used for pretreatment and for finishing ρ_{aoI} and ρ_{aoII}, respectively.

Numerical analyses, presented in this work, showed, that in the case of single-part tooth fillet and tooth fillet with slight undercut at tooth root mainly nominal angle of tooth profile α and radius of curvature of tooth fillet in the critical section ρ_F (related to tip radius of tooth of particular tool used for pretreatment ρ_{aoI}) have the most significant influence on stresses at tooth root. With increasing angle α tooth thickness grows which declines maximum bending stresses at tooth root. Amplification of tip radius of tooth of particular tool used for pretreatment ρ_{aoI} leads to magnification of radius of curvature of tooth fillet in the critical section ρ_{FI}. This also leads to lessening maximum bending stresses at tooth root. In the examples shown in this paper increasing angle of tooth profile α from 15° to 25.0° reduced maximum bending stresses at tooth root by approximately 25% to 30%. The same result was obtained for increasing radius ρ_{aoI} from $\rho_{aoI} = 0$ to $\rho_{aoI} = \rho_{aoI,max}$. Influence of the other considered parameters i.e., number of teeth z and addendum coefficient x was negligible. Changes of these parameters (z, x) caused changes in maximum bending stresses at tooth root (positive or negative) not more than 5%.

In the case of tooth fillet with notch after finishing main geometric parameters of gear tooth i.e., α, z, x influence maximum bending stresses at tooth root in the same way like in the case of single-part tooth fillet. In this case, however, parameters of notch must be taken into account: distance of notch from tooth root h_g, radius of curvature of notch ρ_g (related to tip radius of tooth of particular tool used for finishing ρ_{aoII}) and depth of notch t_g. First of them, distance of notch from tooth root h_g, has the most significant influence on maximum bending stresses at tooth root. Increasing the distance of notch from tooth root h_g can reduce maximum bending stresses at tooth root by approximately 30%. On the other hand it will also lead to shortening of active involute profile at tooth root, which could cause tooth contact interference in

gear transmission. Influence of notch depth t_g was negligible in all considered models. Increase of t_g caused corresponding increase of maximum bending stresses at tooth root not more than 5%. Both notches (after pretreatment and tooth fillet) interact with each other and change of geometric parameters (especially radii of curvature ρ_F or ρ_g) of one of them causes changes in stresses in both of them. Therefore, in the case of type of tooth fillet, considered here, radii of curvature ρ_F or ρ_g must be analyzed together. In most cases optimum values of parameters h_g and ρ_F (depending on ρ_{aoI}) as well as ρ_g (depending on ρ_{aoII}) can be determined. These optimum values lead to minimum bending stresses at tooth root.

Notch after finishing also causes concentration of stresses and, therefore, reduces tooth root strength for bending. However, for certain combinations of geometric parameters of both notches it could also lighten tooth root. Stresses in this notch could be less than stresses at tooth fillet and even less than stresses at tooth root without notch. However, it should be noticed, that this conclusion is based only on analysis of influence of geometric parameters of notch on bending stresses and does not consider influence of finishing, especially grinding, on material properties of outer layer in surrounding of the notch. In result of finishing some negative phenomena (as far as tooth root strength is considered) in this region can turn up: change of structure of outer layer, residual stresses, micro-cracks, reduction of material hardness, etc.

Results of performed investigations show, that in the case when tooth flank and tooth root must be machined in two separate technological operations profitable solution consists in application of tooth fillet with undercut. Small, intentional undercut at tooth root causes small increase of bending stresses at tooth root, compared to single-part tooth fillet, allowing avoiding grinding of tooth root and in consequence of it - avoiding grinding burns in outer layer of tooth root. Major disadvantage of it is relatively high cost (compared to standard generating tools) of manufacturing of special tools with protuberance, necessary for machining of suitable undercut during gear generation in pretreatment. Moreover, in some cases, even if tool with protuberance is used for gear generation in pretreatment, additional geometric notch can appear after finishing, due to: too large deformations of gear after heat treatment, big deviations in pretreatment or deviations in setting of tool for finishing.

Possible good solution consists in replacement of grinding with finishing machining of teeth in hard state, utilizing super-hard materials for tools [4]. However, cost of such tools is currently very high and, therefore, its application in gear manufacturing is still limited.

If additional notch at tooth root cannot be avoided, its negative influence on bending stresses at tooth root should be minimized by suitable selection of its geometric parameters.

Results of computations of stresses at tooth root, obtained with use of the finite element method, were compared with related calculations made in accordance with the procedures given in ISO/DIS and ANSI/AGMA standards

(in the AGMA standard formulas for calculation of root stresses describe only single-part fillet and fillet with undercut). Comparison of the results showed relatively good conformity in the case of single-part fillet. In the case of fillet with notch ISO/DIS-based calculations followed to significantly bigger stresses at tooth root than FEM computations, especially in the case of relatively big distance of notch from tooth root h_g (Fig. 14). This parameter significantly influences bending stresses at tooth root, but is not considered in the ISO/DIS standard (Eq. 16). In calculations of coefficient Y_{sg}, representing concentration of stresses caused by notch, according to the ISO/DIS standard, only depth of notch t_g and its radius of curvature ρ_g are considered.

Presented investigations, utilizing CAE techniques, establish proper basis for optimization of gear design and manufacturing, leading to manufacturing of gears with maximum possible tooth root strength. This optimization takes into account: setting initial structural and technological parameters, computer simulation of gear generation, computer assisted strength analysis leading to suitable modification of design and manufacturing presumptions. The approach presented in this paper can be also useful for strength analysis of other types of machine parts, which contain notches generated during machining and cannot be easily avoided.

<div style="text-align:center">

Manuscript received by Editorial Board, February 08, 2001;
final version, July 31, 2001.

</div>

<div style="text-align:center">

REFERENCES

</div>

[1]   ADINA Theory and modeling guide. ADINA R&D, Inc., Watertown, MA 2000.

[2]   ANSI/AGMA 6002-B93 Standard, Design guide for vehicle spur and helical gears.

[3]   Bathe K.J.: Finite Element Procedures. Prentice Hall, Inc., Englewood Cliffs, NJ, 1996.

[4]   Bausch T. ed.: Moderne Zahnradfertigung. Verfahren Maschinen zur kostengünstigen Herstellung von Stirn- und Kegelrädernmit hoher Qualität. Expert Verlag, Renningen-Malmsheim 1994.

[5]   Brzoska Z.: Wytrzymałość materiałów. PWN, Warszawa 1974.

[6]   DIN 3990, Tragfähigkeitsberechnung von Stirnrädern, Dezember 1987.

[7]   Dietrich M. red.: Podstawy konstrukcji maszyn. Tom IV. PWN, Warszawa 1991.

[8]   Hösel T.: Vergleich genormter Tragfähigkeitsberechnungen für Stirnräder nach AGMA 218.01, DIN 3990, ISO/DIS 6336 und TGL 10 545. Antriebstechnik, 27 (1988) 1, pp. 37÷39.

[9]   Hösel T.: Einfluß der Zahnform auf die Flanken- und Zahnfußtragfähigkeit nach DIN 3990 und AGMA 218.01 - Grenzen für Optimierungsrechnungen. Antriebstechnik, 27 (1988) 9, pp. 65÷68.

[10]   Hösel T.: Vergleich der Tragfähigkeitsberechnungen für Stirnräder nach ANSI/AGMA, ISO/DIN- und RGW-Normen. Antriebstechnik, 28 (1989) 11, pp. 77÷84.

[11]   ISO/DIS 6336 Standard, Calculation of Load Capacity of Spur and Helical Gears.

[12]   Jaśkiewicz Z., Wąsiewski A.: Przekładnie walcowe. WKiŁ, Warszawa 1992.

[13] Kawalec A.: Modelling of tooth flanks based on distorted measurements. Advances in Technology of Machines and Mechanical Equipment, 21 (1997) 3, pp. 5÷28.

[14] Kawalec A.: An influence of load distribution on stresses and deformations of tooth in straight-tooth spur gear transmission. Advances in Technology of the Machines and Equipment, 22 (1998) 3, pp. 53÷77.

[15] Kawalec A., Wiktor J.: Analytical and numerical method of determination of spur gear tooth profile machined by gear tools. Advances in Technology of the Machines and Equipment, 23 (1999) 2, pp. 5÷28.

[16] Kleiber M. ed.: Handbook of Computational Solid Mechanics. Springer, Berlin 1998.

[17] Linke H.: Spannungkonzentration bei Verzahnungen. Maschinenbautechnik, 32 (1983) 4, pp. 174÷179.

[18] Linke H., Sporbert K.: Einfluß des Schleifabsatzes auf die Spannungkonzentration bei Verzahnungen. *Maschinenbautechnik*, 34 (1985) 4, pp. 251÷257.

[19] Niemann G., Winter H.: Maschinenelemente, Band II. Springer Verlag, Berlin 1985.

[20] Townsend D.P.: Dudley's Gear Handbook. McGraw-Hill, Inc., New York 1992.

[21] Weck M.: Moderne Leistungsgetriebe. Verzahnungsauslegung und Betriebsverhalten. Springer Verlag, Berlin 1992.

[22] Wiktor J.: Sztywność zazębienia ewolwentowych przekładni walcowych. Przegląd Mechaniczny, 54 (1995) 20, pp. 17÷21.

[23] Winter H., Hirt M.: Zahnfußtrgfähigkeit auf der Grundlage der wirklichen Spannungen. Spannungskorrekturfaktor, Kerbempfindlichkeitszahl und relativer Kerbfaktor in ISO-Ansatz. *VDI-Z*, 116 (1974) 2, pp.119÷126.

[24] Winter H., Straßer H.: Auswirkung der Kerbempfindlichkeit von Werkstoffen auf Zahnfußtragfähigkeit nach DIN 3990. Antriebstechnik, 23 (1984) 3, pp. 49÷56.

[25] Życzkowski M. ed.: Strength of Structural Elements. PWN, Elsevier, Warszawa, Amsterdam 1991.

Analiza wytrzymałości podstawy zęba z karbem po obróbce wykańczającej w ewolwentowych uzębieniach walcowych

Streszczenie

W pracy wykorzystano komputerową symulację obwiedniowej obróbki walcowych ewolwentowych kół zębatych. Symulacja posłużyła do wyznaczenia zarysów zębów odwzorowywanych przez narzędzia w trakcie procesu wytwarzania kół zębatych. Zarysy zębów obliczono dla różnych kombinacji parametrów geometrycznych wytwarzanych kół zębatych i narzędzi, oraz różnych wariantów skojarzenia obróbki wstępnej i wykańczającej. Rezultaty tych obliczeń wykorzystano do budowy bardzo precyzyjnych modeli odpowiednich segmentów kół zębatych przeznaczonych do analizy metodą elementów skończonych. Rozkłady naprężeń w tych modelach obliczono z wykorzystaniem systemu MES ADINA. Wyniki porównano z odpowiednimi wynikami obliczeń przeprowadzonych w oparciu o normy ISO/DIS i AGMA. Szczególną uwagę zwrócono na koła z karbem powstającym w wyniku obróbki u podstawy zęba. Taki karb jest przyczyną koncentracji naprężeń. Obliczenia przeprowadzone na ww. modelach pozwoliły przeanalizować wpływ parametrów technologicznych oraz metod obróbki na kształt i wytrzymałość na zginanie podstawy zęba walcowych kół zębatych. Sformułowano generalne wnioski wynikające z ww. analizy. Mogą być one pomocne w projektowaniu i wytwarzaniu kół zębatych, we właściwym wyborze parametrów konstrukcyjnych, kojarzeniu obróbki wstępnej

i wykańczającej, oraz w doborze odpowiedniej metody wytwarzania i parametrów stosowanego narzędzia. Podejście zaproponowane w tym artykule, polegające na przyjęciu wstępnych parametrów konstrukcyjnych i technologicznych oraz komputerowo wspomaganej analizie wytrzymałościowej – prowadzącej do stosownej modyfikacji założeń konstrukcyjnych i technologicznych, stanowi dobrą podstawę do optymalizacji kół zębatych, uwzględniającej maximum wytrzymałości na zginanie podstawy zęba walcowych kół zębatych.